A Josephson radiation comb generator

P. Solinas,[1,*] S. Gasparinetti,[2,3] D. Golubev,[3,4] and F. Giazotto[5,†]

[1]SPIN-CNR, Via Dodecaneso 33, 16146 Genova, Italy
[2]Department of Physics, ETH Zürich, CH-8093 Zürich, Switzerland
[3]Low Temperature Laboratory (OVLL), Aalto University School of Science, P.O. Box 13500, 00076 Aalto, Finland
[4]Institute of Nanotechnology, Karlsruhe Institute of Technology, D-76021 Karlsruhe, Germany
[5]NEST, Instituto Nanoscienze-CNR and Scuola Normale Superiore, I-56127 Pisa, Italy

Optical frequency combs have been a major research trend of the last decade [1]. The possibility to generate higher harmonics starting from a fundamental one has made it possible to extend the accuracy of the atomic clocks from the radio to the optical frequency region, leading to breakthroughs in optical metrology [2], high precision spectroscopy [3, 4] and telecommunication technologies [1, 5]. Here we show that a similar-in-spirit harmonic generator can be implemented with a dc superconducting quantum interference device (SQUID) subject to a time-dependent magnetic field. Driven by the field, the superconducting phase difference across the SQUID undergoes jumps of π, which are associated to a sequence of sharp, evenly spaced voltage pulses. This pulse sequence translates into a radiation comb in frequency domain, thereby realizing a Josephson radiation comb generator (JRCG). Under suitable conditions, the JRCG can provide up to several hundreds of harmonics of the driving frequency. For example, a chain of 10^4 identical high-critical-temperature SQUIDs driven at 1 GHz can deliver up to a few tens nW at 500 GHz. The availability of a fully solid-state radiation comb generator such as the JRCG, easily integrable on chip, will pave the way to a number of technological applications, from metrology to sub-millimeter wave generation.

Our proposal for a JRCG is based on a dc SQUID (see Fig. 1a), consisting of two Josephson junctions arranged in parallel in a superconducting loop. The SQUID is biased by a constant current I_B and it is driven by an external, time-dependent magnetic flux Φ. Here we assume the inductance of the loop to be negligible with respect to the Josephson inductance of the junctions. Due to the first Josephson relation [6], the current (I_J) vs phase relation of the SQUID reads

$$I_J(\varphi;\phi) = I_+[\cos\phi\sin\varphi + r\,\sin\phi\cos\varphi], \qquad (1)$$

where $\varphi = (\varphi_1+\varphi_2)/2$, $\phi = \pi\Phi/\Phi_0$ ($\Phi_0 \simeq 2\times10^{-15}$ Wb is the flux quantum), $I_+ = I_{c1}+I_{c2}$, φ_i and I_{ci} ($i=1,2$) are the phase across and the critical current of the i-th junction, respectively, and $r = (I_{c1}-I_{c2})/(I_{c1}+I_{c2})$ expresses the degree of asymmetry of the interferometer. Equation (1) describes the well-known oscillations of the SQUID critical current $I_c(\phi) = \max_\varphi I_J(\varphi;\phi)$ as a function of the magnetic flux, with minima occurring at integer multiples of $\Phi_0/2$ (see Fig. 1b) [6], and it already contains the main feature of the effect we want to discuss. Let us consider the behavior of the phase φ as Φ crosses a critical-current minimum and take a symmetric SQUID ($r=0$) for simplicity. If the biasing current is fixed, then we see from Eq. (1) that a change of sign in $\cos\phi$ must be accompanied by a change of sign in $\sin\varphi$ in order for the current to maintain its direction. This change of sign is accomplished by a phase jump of π [7–9], which, owing to the second Josephson relation [6], results in a voltage pulse $V(t)$

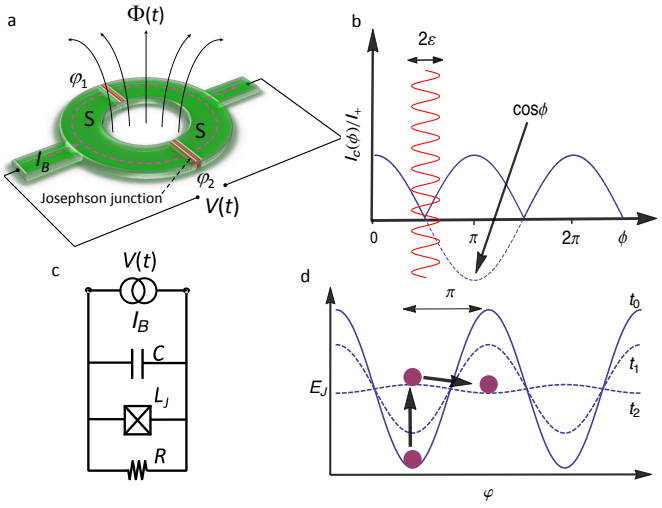

FIG. 1: **The Josephson radiation comb generator.** a) Sketch of the dc SQUID subject to a time-dependent magnetic flux $\Phi(t)$. The latter induces voltage pulses $V(t)$ across the interferometer. The red regions denote the two Josephson tunnel junctions, I_B is the SQUID constant bias current, φ_i is the phase across the i-th junction, and S are the superconducting electrodes. b) Interference pattern of the critical current $I_c(\phi)$ (where $\phi = \pi\Phi/\Phi_0$) for a symmetric SQUID ($r=0$). $I_c(\phi)$ is plotted with solid line while the ϕ-dependent part, i.e., $\cos\phi$, is plotted with dashed line. The phase φ undergoes a π jump whenever ϕ crosses an interference node as the $\cos\phi$ becomes negative. Red line shows $\phi(t)$ oscillating with frequency ν and amplitude ε around an interference node at $\pi/2$. $\phi(t)$ induces dynamically the phase jumps in the SQUID. c) RCSJ model circuit where R, L_J, C are the resistance, the Josephson inductance and the capacitance of the SQUID, respectively. d) Time-dependent tilted-washboard Josephson potential for the RCSJ model plotted for $t_0=0$, at an intermediate time $t_1 = 0.17/\nu$, and at $t_2 = 0.26/\nu$ just after vanishing of the potential barrier, i.e., the $E_J = -E_{J0}\delta\varphi$ point. The system is initially (i.e., at $t_0=0$) in an energetic minimum with phase $\varphi = 2k\pi$. Because of the drive, the potential vanishes at time $1/(4\nu)$. Then, the system reaches a potential maximum and jumps into the nearest minimum at $\varphi = (2k+1)\pi$. The direction of the jump is determined by the direction of I_B. The latter is supposed to be small with respect to I_+.

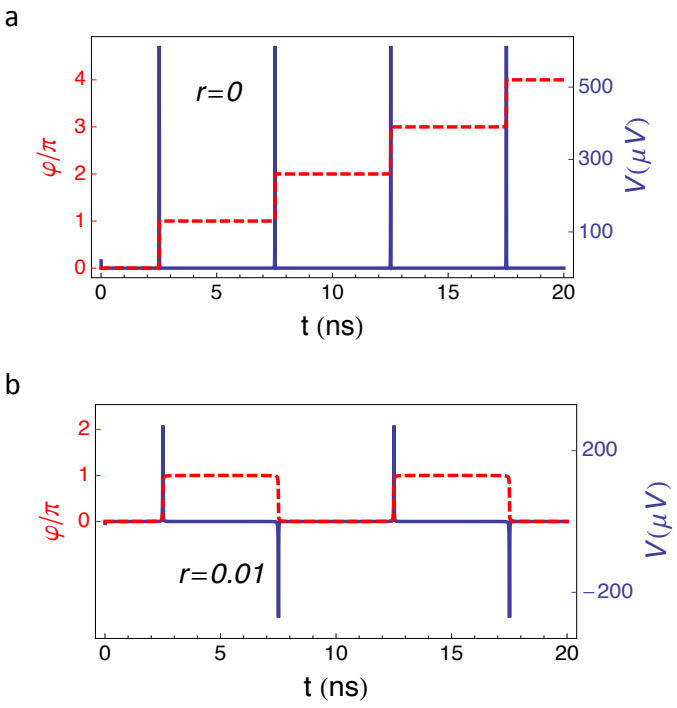

FIG. 2: **Phase jumps and voltage combs.** Time dependence of the phase φ (dashed line, left axis) and of the voltage V (solid line, right axis) across a flux-driven SQUID. The driving frequency is $\nu = 100$MHz. a) Symmetric SQUID ($r = 0$) and $I_B = 10^{-3} I_+$. The direction of the phase jumps is determined by the bias current. b) Asymmetric SQUID ($r = 0.01$) and $I_B = 0$. The SQUID asymmetry induces alternate phase jumps even in the absence of an external biasing current. One-directional jumps can be realized by applying a suitable I_B. The voltage pulses are generated at times $(2k+1)/4\nu$ (with k integer) when the interference node is crossed. The parameters chosen for the calculations are those typical of a Nb/AlOx/Nb junction [10] with $R = 20$ Ohm, $I_+ = 0.2$ mA, and we set $\varepsilon = 0.9$. The typical junction capacitance, $C = 10$ fF, has been neglected (as additional numerical simulations show).

across the SQUID.

For a quantitative characterization of the phase jumps, we need to study the dynamics of the phase. To do so, we rely on the resistively and capacitively shunted Josephson junction (RCSJ) model [6, 11]. We model the SQUID as a capacitor C, a resistor R, and a non-linear, flux-dependent inductor L_J arranged in a parallel configuration (see Fig. 1c). We consider a sinusoidally-driven magnetic flux with frequency ν and amplitude ε, centered in the first node of the interference pattern, so that $\Phi(t) = \Phi_0/2[1 - \varepsilon\cos(2\pi\nu t)]$. As a result, the magnetic flux crosses the nodes of the interference pattern at $t = (2k+1)/4\nu$, with k integer. The equation for φ can be written in terms of the dimensionless variable $\tau = 2\pi\nu t$ as [11]

$$c\frac{d^2\varphi}{d\tau^2} + \frac{d\varphi}{d\tau} + \alpha[f(\varphi,\tau) - \delta] = 0, \qquad (2)$$

where $\delta = I_B/I_+$, $c = 2\pi RC\nu$, $f(\varphi,\tau) = I_J[\varphi;\phi(\tau)]/I_+$ and $\alpha = I_+ R/(\Phi_0\nu)$.

Equation 2 is usually interpreted in terms of a fictitious phase particle moving in a tilted-washboard Josephson potential E_J, as shown in Fig. 1d [6]. Here we restrict ourselves to small biasing current ($\delta \ll 1$), corresponding to a small tilt. Furthermore, we focus on the limits $c \ll 1$ (*overdamped* regime) and $|\alpha| \gg 1$, as these two conditions maximize the JRCG performance (see SI).

We first consider a symmetric SQUID ($r = 0$). Then the time-dependent Josephson potential is $E_J(t) = \int I_{tot} V(t) dt = -E_{J0}[f(t)\cos\varphi + \delta\varphi]$ where $f(t) = \cos(\pi\Phi/\Phi_0)$, $E_{J0} = \Phi_0^2\nu\alpha/(2\pi R)$, and $I_{tot} = I_J - I_B$ [6, 11]. At $t = 0$ it has minima at $\varphi = 2k\pi$. For $t = 1/(4\nu)$ the potential barrier vanishes and $E_J = -E_{J0}\delta\varphi$. For $t > 1/(4\nu)$, $f(t)$ changes sign and the potential minima occur at $\varphi = (2k+1)\pi$. At $\varphi = 2k\pi$ the system is unstable and tends to move to a new minimum, resulting in a π-jump in the phase. This cartoon picture helps us to pinpoint the difference between the phase jumps discussed in this work, the 2π-phase slips appearing in low-dimensional superconductors [12–15] and the 2π-phase jumps used in the rapid single flux quantum (RSFQ) logic [16, 17]. 2π-phase slips typically stem from thermal activation or quantum fluctuations. As for the RSFQ 2π-phase jumps, they are generated by a current pulse in an otherwise static potential landscape. By contrast, in the JRCG the magnitude of the jumps is π and the jumps have a purely energetic origin.

The numerical solution of Eq. (2) for $r = 0$ is shown in Fig. 2a. As the critical current crosses the minimum at $\Phi = \Phi_0/2$, the phase experiences a π jump and a voltage pulse is generated across the SQUID. The shape of the pulse is determined by the parameter α (see SI): the *larger* α, the *sharper* the voltage pulse. We notice that the presence of a finite bias current I_B is crucial to impose a preferred direction to the phase jumps. The same analysis essentially holds as well for a weakly-asymmetric SQUID ($r \ll 1$), as long as I_B is strong enough to force the phase particle to roll always in the same direction. However, the junctions asymmetry brings in a key ingredient to the JRCG, which becomes apparent in the limit $I_B \to 0$. Indeed, a finite SQUID asymmetry imposes an alternate pattern to the phase jumps (see Fig. 2b and SI). This realizes an ideal ac pulse source. Furthermore, the limit $I_B \to 0$ corresponds to a floating device, meaning that the ac JRCG can be straightforwardly integrated in microwave-based architectures such as circuit-QED [18–20].

The voltage pulses shown in Fig 2 suggest an application similar to the frequency combs used in optics [1]. In this context, the most relevant feature becomes the sharpness of the voltage pulse, which is related to the number of harmonics generated. The sharpness is essentially determined by α, which, in turn, depends on the material properties of the Josephson junctions as well as on the driving frequency. In Figure 3 we show the calculated JRCG power spectrum P vs frequency Ω (see SI) for two driving frequencies and for different junctions and symmetry parameters. While the total output power provided by a single JRCG is fairly small, it can be boosted by using an array of nominally-identical SQUIDs. A similar approach is used for the realization of the metrolog-

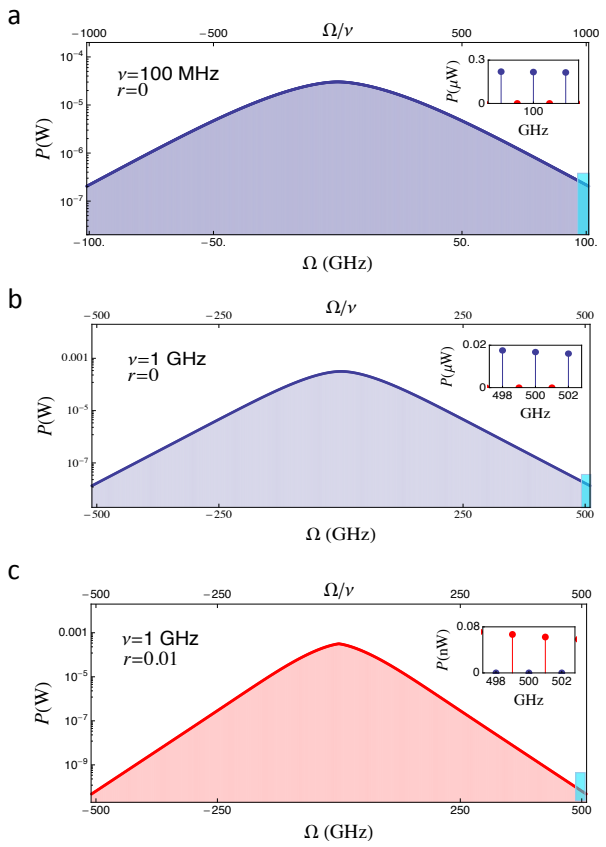

FIG. 3: **Power spectrum of the Josephson radiation comb generator coupled to a 50 Ohm transmission line**. To emphasize the behavior at high frequency we use a logarithmic scale in the main panels but keep the linear scale in the insets. The cyan regions correspond to the insets. (a) Behavior of the power spectrum P vs frequency Ω for a symmetric ($r = 0$) Nb/AlOx/Nb SQUIDs chain subject to a driving frequency $\nu = 100$ MHz. The SQUID parameters were set as those in Fig. 2. In the calculation the junction capacitance has been neglected since it does not affect the dynamics. The inset shows that an output power of ~ 0.3 μW around 100 GHz (10^3-th harmonic) can be achieved. (b) Behavior of P vs Ω for a symmetric ($r = 0$) high-critical temperature YBCO SQUIDs chain subject to a driving frequency $\nu = 1$ GHz. The inset shows P around 500 GHz (500-th harmonic) where ~ 20 nW can be achieved. Here we set $I_+R = 10$ mV and $I_B = 10^{-3}I_+$ [21, 22]. The junction capacitance is typically very small in this kind of junctions, $C \sim$ fF, and has been neglected in the calculations. (c) Behavior of P vs Ω for an asymmetric ($r = 0.01$) YBCO SQUIDs chain and $\nu = 1$ GHz. Here we set $I_+R = 10$ mV and $I_B = 0$. In all calculations Φ oscillates around the first interference node ($\Phi_0/2$) with elongation $\varepsilon = 0.9$. Blue and red point indicate the even and odd harmonics, respectively. In Figs. a and b only the *even* harmonics are present because of the comb-like shape of the voltage pulses. In Fig. c, due to the alternating direction of the voltage pulses, only the *odd* harmonics are present. In this latter case, the output power at high frequency is smaller.

ical standard for voltage based on the Josephson effect [23–25]. For an array of N SQUIDs, the output power scales as N^2 allowing one to reach a sizable output power at high frequency. Here we present results for $N = 10^4$ [11, 26, 27]. Figure 3a displays the behavior of a symmetric Nb/AlOx/Nb SQUIDs chain [10] with a 100 MHz drive. The parameters are the same as those in Fig. 2a. The sharp pulses determine the broad range of the emitted radiation, up to several hundreds of harmonics. At 100 GHz (see the inset of Fig. 3a) the JRCG provides an output power of $\sim 0.3\,\mu$W. This power level can be detected, for instance, by coupling the device to a transmission line and feeding the signal to a commercial spectrum analyzer.

In order to achieve sharp pulses at higher frequencies, one needs to use a superconductor with a larger characteristic voltage (I_+R). In such a way, one can drive the SQUID at higher frequencies without lowering α. In Fig. 3b we show the results expected for a symmetric high-critical temperature YBCO SQUIDs series [21, 22] at 1 GHz drive. YBCO Josephson junctions provide a large superconducting gap with $I_+R \approx 10$ mV and possess a negligible intrinsic capacitance [22]. Due to the larger driving frequency, the emitted signal at 500 GHz is still sizable, reaching an output power of a few tens of nW (see the inset of Fig. 3b). Such a signal is already in the far infrared range, which has seen a substantial research development in the last two decades due to countless technological applications. The radiated signal in this frequency range could be detected, for instance, by using an antenna coupled to the SQUID electrodes [28, 29]. The power spectrum of an asymmetric YBCO SQUIDs chain is similar (see Fig. 3c). The main differences lie in the presence of *odd* harmonics only and in a smaller output power at high frequency (~ 0.1 nW around 500 GHz, see the inset of Fig. 3c).

Let us briefly address some experimental issues related to the JRCG. We have analyzed the effect of thermal noise at 4.2 K on the device performance. Noise is expected to be the most harmful in the vicinity of the phase jumps, as the potential barrier is the most shallow there (see Fig. 1d). However, our numerical calculations (see SI) show that its effect is negligible for the parameters used in Fig. 3. Thermal noise could play a role at slow driving frequencies because it is easier to induce undesired transitions when the the potential barrier is shallow. However, this effect can be counteracted by increasing the current I_B to impose a privileged direction to the dynamics (see SI).

The proposed JRCG is within the reach of state-of-the-art nanofabrication technology. SQUID arrays with an asymmetry dispersion of the order of $\sim 0.05 - 1\%$ can be fabricated with standard lithographic techniques. Furthermore, a single on-chip superconducting line can be used to drive the magnetic fluxes of a SQUID array in a synchronized manner and with ns time resolution. Finally, the fact that the JRCG is operated in the overdamped regime means that it can be designed to have a low output impedance. The latter can be easily matched to that of a transmission line (50 Ohm) or of a superconducting antenna. The implementation of the JRCG will pave the way to a number of applications, from low-temperature microwave electronics to on-chip sub-millimiter wave generation.

We gratefully acknowledge M. Hofheinz, M. J. Martínez-

Pérez, M. Pechal, A. Tredicucci for fruitful discussions. P.S. has received funding from the European Union FP7/2007-2013 under REA grant agreement no 630925 – COHEAT and from MIUR-FIRB2013 – Project Coca (Grant No. RBFR1379UX). The work of F.G. was partially supported by the Marie Curie Initial Training Action (ITN) Q-NET 264034, and by the European Research Council under the European Union's Seventh Framework Programme (FP7/2007-2013)/ERC grant agreement No. 615187-COMANCHE. S.G. acknowledges financial support from the Aalto University network in Condensed Matter and Materials Physics (CMMP) and from the Swiss National Science Foundation (SNF) Project 150046.

* Electronic address: paolo.solinas@spin.cnr.it
† Electronic address: giazotto@sns.it

[1] Udem, T., Holzwarth, R. & Hänsch, T. W. Optical frequency metrology. *Nature* **416**, 233–237 (2002).
[2] Hänsch, T. & Walther, H. Laser spectroscopy and quantum optics. *Reviews of Modern Physics* **71**, S242 (1999).
[3] Bloembergen, N. *Nonlinear spectroscopy*, vol. 64 (North Holland, 1977).
[4] Hänsch, T. W. & Inguscio, M. *Frontiers in Laser Spectroscopy: Varenna on Lake Como, Villa Monastero, 23 June-3 July 1992*, vol. 120 (North Holland, 1994).
[5] Foreman, S. M., Holman, K. W., Hudson, D. D., Jones, D. J. & Ye, J. Remote transfer of ultrastable frequency references via fiber networks. *Review of Scientific Instruments* **78**, 021101 (2007).
[6] Tinkham, M. *Introduction to superconductivity* (Courier Dover Publications, 2012).
[7] Giazotto, F. & Martínez-Pérez, M. J. The Josephson heat interferometer. *Nature* **492**, 401–405 (2012).
[8] Giazotto, F., Martínez-Pérez, M. & Solinas, P. Coherent diffraction of thermal currents in Josephson tunnel junctions. *Physical Review B* **88**, 094506 (2013).
[9] Martínez-Pérez, M. J. & Giazotto, F. A quantum diffractor for thermal flux. *Nature communications* **5** (2014).
[10] Patel, V. & Lukens, J. Self-shunted Nb/AlO/sub x//Nb Josephson junctions. *Applied Superconductivity, IEEE Transactions on* **9**, 3247–3250 (1999).
[11] Gross, R. & Marx, A. Applied superconductivity: Josephson effect and superconducting electronics. *Walther-Meißner-Institut, Walther-Meißner-Str* **8**, 85748 (2005).
[12] Arutyunov, K. Y., Golubev, D. S. & Zaikin, A. D. Superconductivity in one dimension. *Physics Reports* **464**, 1–70 (2008).
[13] Astafiev, O. *et al.* Coherent quantum phase slip. *Nature* **484**, 355–358 (2012).
[14] Langer, J. S. & Ambegaokar, V. Intrinsic resistive transition in narrow superconducting channels. *Physical Review* **164**, 498 (1967).
[15] Zaikin, A. D., Golubev, D. S., van Otterlo, A. & Zimanyi, G. T. Quantum phase slips and transport in ultrathin superconducting wires. *Physical review letters* **78**, 1552 (1997).
[16] Likharev, K., Mukhanov, O. & Semenov, V. Resistive single flux quantum logic for the Josephson-junction digital technology. *Proc. SQUID'85* 1103–1108 (1985).
[17] Mukhanov, O., Semenov, V. & Likharev, K. Ultimate performance of the RSFQ logic circuits. *Magnetics, IEEE Transactions on* **23**, 759–762 (1987).
[18] Blais, A., Huang, R.-S., Wallraff, A., Girvin, S. & Schoelkopf, R. J. Cavity quantum electrodynamics for superconducting electrical circuits: An architecture for quantum computation. *Physical Review A* **69**, 062320 (2004).
[19] Wallraff, A. *et al.* Strong coupling of a single photon to a superconducting qubit using circuit quantum electrodynamics. *Nature* **431**, 162–167 (2004).
[20] Koch, J. *et al.* Charge-insensitive qubit design derived from the Cooper pair box. *Physical Review A* **76**, 042319 (2007).
[21] Malnou, M. *et al.* Josephson mixers for terahertz detection. *arXiv preprint arXiv:1405.5998* (2014).
[22] Rosenthal, P. & Grossman, E. N. Terahertz Shapiro steps in high temperature SNS Josephson junctions. *Microwave Theory and Techniques, IEEE Transactions on* **42**, 707–714 (1994).
[23] Shapiro, S. Josephson currents in superconducting tunneling: The effect of microwaves and other observations. *Physical Review Letters* **11**, 80 (1963).
[24] Kautz, R. & Lloyd, F. L. Precision of series-array Josephson voltage standards. *Applied physics letters* **51**, 2043–2045 (1987).
[25] Tsai, J.-S., Jain, A. & Lukens, J. High-precision test of the universality of the Josephson voltage-frequency relation. *Physical review letters* **51**, 316 (1983).
[26] Lloyd, F. L. *et al.* A Josephson array voltage standard at 10 V (1987).
[27] Pöpel, R., Niemeyer, J., Fromknecht, R., Meier, W. & Grimm, L. 1-and 10-V series array Josephson voltage standards in Nb/Al2O3/Nb technology. *Journal of applied physics* **68**, 4294–4303 (1990).
[28] Vicarelli, L. *et al.* Graphene field-effect transistors as room-temperature terahertz detectors. *Nature materials* **11**, 865–871 (2012).
[29] Erickson, R. P., Vissers, M. R., Sandberg, M., Jefferts, S. R. & Pappas, D. P. Ultra-Broadband Microwave Frequency-Comb Generation in Superconducting Resonators. *arXiv preprint arXiv:1405.7117* (2014).

SUPPLEMENTARY INFORMATION

SOLUTION OF THE RCSJ EQUATION IN A DC SQUID

We consider a dc SQUID composed by two Josephson junctions and subject to a magnetic flux Φ. The total current though the SQUID is $I_J = I_{c1}\sin\varphi_1 + I_{c2}\sin\varphi_2$, where I_{ci} and φ_i are the critical current and the phase across the i-th junction, respectively. Because of the flux quantization constraint, it follows that $(\varphi_1-\varphi_2)/2 = \pi\Phi/\Phi_0$. Introducing the phase across the SQUID $\varphi = (\varphi_1+\varphi_2)/2$, we get

$$I_J[\varphi;\phi(\tau)] = I_+[\cos\phi\sin\varphi + r\ \sin\phi\cos\varphi], \tag{1}$$

where $\phi = \pi\Phi/\Phi_0$, $I_+ = I_{c1}+I_{c2}$, $r = (I_{c1}-I_{c2})/(I_{c1}+I_{c2})$ and $\Phi_0 \simeq 2\times10^{-15}$ Wb is the flux quantum.

Starting from the RCSJ model [6, 11], we can write an equation of motion for the phase φ as

$$\frac{\hbar C}{2e}\ddot{\varphi} + \frac{\hbar}{2eR}\dot{\varphi} + I_+ f(\varphi,t) = I_B \tag{2}$$

where C is the capacitance, R is the total shunting resistance of the SQUID, I_B is the external biasing current and $f(\varphi,t) = I_J[\varphi;\phi(t)]/I_+$. We rescale the above equation in terms of the driving frequency ν: $\tau = 2\pi\nu t$. Using $\hbar/(2e) = \Phi_0/(2\pi)$, we obtain

$$c\frac{d^2\varphi}{d\tau^2} + \frac{d\varphi}{d\tau} + \alpha[f(\varphi,\tau)-\delta] = 0, \tag{3}$$

where $\delta = I_B/I_+$, $c = 2\pi RC\nu$ and

$$\alpha = \frac{I_+R}{\Phi_0\nu}. \tag{4}$$

Analytical solution for $I_B = 0$

Let us consider the case of a symmetric dc SQUID ($r=0$), overdamped junctions ($c\approx 0$) and zero current bias ($\delta = 0$). Then (3) reduces to

$$\frac{d\varphi}{d\tau} + \alpha f(\tau)\sin\varphi = 0. \tag{5}$$

We notice that if the initial condition is $\varphi(0) = \varphi_0 = k\pi$, the above equation has trivial dynamics $\varphi(t) = 0$. This means that, even if small, we cannot neglect the influence of the $\ddot{\varphi}$ term. However, if $\varphi_0 \neq k\pi$, we can effectively neglect the capacitive contribution and solve analytically the differential equation (2) to obtain

$$\varphi(t) = 2\arctan\left[\exp\left(-\alpha\int_0^t d\tau f(\tau)\right)\tan\frac{\varphi_0}{2}\right]. \tag{6}$$

We suppose that $|\alpha| \gg 1$ (and $\alpha > 0$). If $\int_0^t d\tau f(\tau)$ assumes positive and negative values, the argument of *arctan* increases or decreases exponentially depending on its sign. For simplicity, we consider $\int_0^t d\tau f(\tau) < 0$ and the case of small φ_0. For $\varphi_0 > 0$, $\varphi(t)$ exponentially reaches π, and for $\varphi_0 < 0$, the evolution is similar but $\varphi(t)$ varies between φ_0 and $-\pi$. Therefore, in both cases we have an exponential π jump of the phase but its direction is determined by the initial phase φ_0. The rate of the exponential jump is determined by α: the larger α, the sharper the voltage pulse.

Recalling the phase particle analogy discussed in the main text, with $c = 0$ if the phase is initially in the minimum $\varphi_0 = 2k\pi$ it will remains in the same point even when it becomes an unstable maximum. A small shift of the initial condition induces an exponential dynamics since at $t = 1/(4\nu)$ the phase is close to (but not on) a potential maximum. The direction of this shift (and, in the case discussed, the sign of φ_0) determines the direction of the fall and the jump of the phase.

The change in time of φ in Eq. (6) is associated to a voltage

$$\frac{2e}{\hbar}V(t) = \frac{-\alpha f(t)\sin\varphi_0}{\sin^2\left(\frac{\varphi_0}{2}\right)e^{-\alpha\int_0^t f(\tau)d\tau} + \cos^2\left(\frac{\varphi_0}{2}\right)e^{\alpha\int_0^t f(\tau)d\tau}} \tag{7}$$

For $\varphi_0 \ll 1$, this can be approximated with

$$\frac{2e}{\hbar}V(t) \approx -\alpha f(t)\varphi_0 e^{-\alpha\int_0^t f(\tau)d\tau} \tag{8}$$

which points out the exponential increase of the voltage. The full analytical behavior of $V(t)$ is not easy to obtain from Eq. (7), and we have to use a numerical approach.

Solution for $I_B \neq 0$

We consider now the case of a small biasing current I_B in a symmetric SQUID ($r=0$). By "small biasing current", we mean that its effect must be negligible with respect to the driven dynamics, i.e., $\delta \ll \alpha$, but must dominate the capacitor dynamics, i.e., $\delta \gg c$.

When $\varphi \approx k\pi$, the Josephson current contribution $\alpha f(\tau)\sin\varphi$ is small and the dynamics is determined only by I_B. Equation (2) reduces to

$$\frac{d\varphi}{d\tau} - \alpha\delta = 0. \tag{9}$$

Away from $\varphi \approx k\pi$, the Josephson current contribution dominates and, therefore, the equation for motion approximatively reads

$$\frac{d\varphi}{d\tau} + \alpha f(\tau)\sin\varphi(\tau) = 0. \tag{10}$$

Since the behavior of $\varphi(t)$ under these two different dynamics is drastically different (linear versus exponential change), we can tune the system parameters in order to effectively separate the two regimes governed by Eqs. (9) and (10) and generate the sequence of exponential phase jumps.

In other terms, the presence of a current bias has two effects. The first is to transport the system away from the region

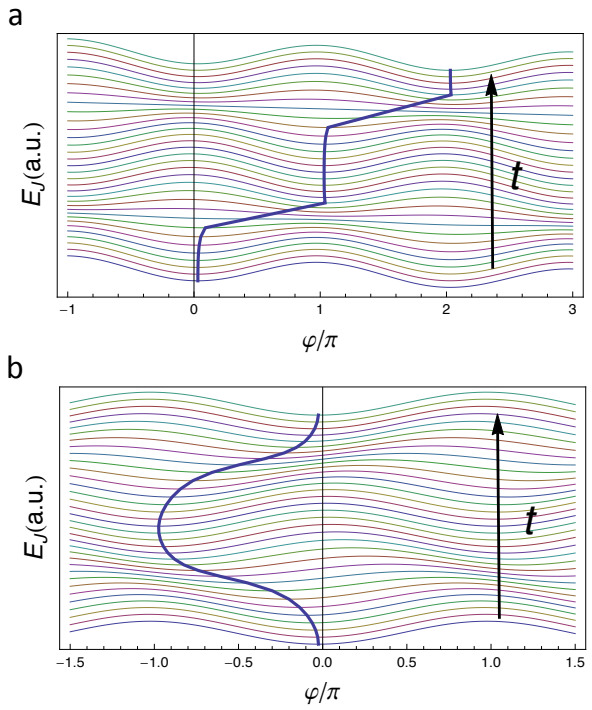

FIG. 1: **Tilted-washboard potential for a symmetric and an asymmetric SQUID.** The energy potential E_J is plotted as a function of φ for different times t. E_J is vertically offset for clarity. The blue curves represent the position of the local minima changing in time. a) Symmetric SQUID, i.e., $r = 0$, with tilt $\delta = 0.3$. The minima are calculated considering the dynamics of the phase particle. b) Asymmetric SQUID with $r = 0.5$ and $\delta = 0$. The energy minimum oscillates back and forth. For presentation purposes both the tilting and the asymmetry parameters are larger than those used in the numerical calculations. The strong tilting produces a small shift in the position of the minima with respect to $k\pi$.

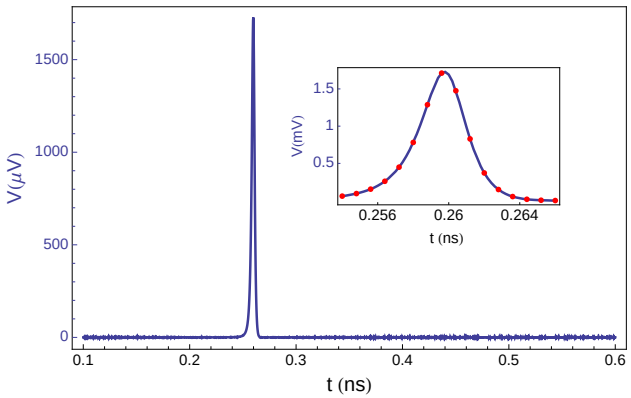

FIG. 2: **Effect of thermal noise on the JRCG dynamics.** Voltage V developed across the SQUID (solid line) as a function of time t in the presence of thermal noise. Here we set the driving frequency to 1 GHz. (Inset) Comparison between noisy (solid line) and noise-free dynamics (red dots). The parameters chosen are those typical of a YBCO junction, as reported in Refs. [21, 22]: $I_+R = 10$ mV, $I_B = 10^{-3}I_+$ and $\varepsilon = 0.9$. The junctions capacitance is negligible and was set to zero. The temperature of the thermal bath is 4.2 K.

$\varphi \approx k\pi$ in which the drive contribution is small and the dynamics is dominated by the capacitive term. The second is to breaks the symmetry of the system inducing the jumps always in the same direction.

The effect of a current bias can be interpreted in terms of the tilted-washboard potential discussed in the main text. In Fig. 1a we show the potential E_J vs φ for different times under a periodic drive. The solid line represents the position of the minima followed by the phase particle in order to minimize the energy.

Asymmetric SQUID case

From Eq. (1), the energy potential reads (we neglect the current bias and set $\delta = 0$) [6]

$$E_J(t) = -E_{J0}(\cos\phi\cos\varphi - r\sin\phi\sin\varphi). \qquad (11)$$

To find the position of the maxima and the minima we derive $E_J(t)$ with respect to ϕ and equal it to zero. The corresponding equation reads $\tan\varphi = \tan(r\phi)$. For $r = 0$, we see that the values of φ satisfying the above equation do not depend on time. On the contrary, for any $r \neq 0$ they depend on time through ϕ .

Following the analogy with the phase particle in a time-dependent potential discussed in the main text, this means that if the system starts in a minimum at $t = 0$, it is close but not in a maximum when the time-dependent potential changes sign. This small perturbation from the stable maximum point induces the phase particle rolling and the corresponding phase jump even in absence of I_B.

For a periodic drive, the particle is found alternatively on the left and on the right of the maximum and it rolls in alternate directions producing the alternate pattern of the voltage pulses. In Fig. 1b, we show the potential E_J vs φ at different times. The solid line represent the position of the minima of the potential. In the absence of a biasing current, the phase must undergo a sequence of positive and negative jumps resulting in the alternate voltage pulses.

EFFECT OF THERMAL NOISE

Langevin approach

To estimate the effect of the thermal noise we use the Langevin equation

$$\frac{\hbar C}{2e}\ddot{\varphi} + \frac{\hbar}{2eR}\dot{\varphi} - I_+ f(t)\sin\varphi = I_B + \xi(t), \qquad (12)$$

where $\xi(t)$ is the white noise with correlation function

$$\langle \xi(t)\xi(t')\rangle = \frac{2k_BT}{R}\delta(t-t'). \qquad (13)$$

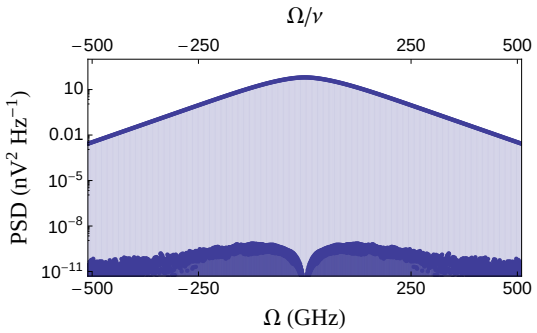

FIG. 3: **Effect of thermal noise on the power spectral density.** Power Spectral Density (PSD) for a YBCO SQUID with 1 GHz drive. Even at high frequency (500 GHz), the signal to noise ratio is about 10^7. Notice that here the PSD is calculated for a single SQUID. For the calculations we set the following parameters [21, 22]: $I_+R = 10$ mV and $I_B = 10^{-3}I_+$. The Josephson junctions capacitance is typically very small, $C \sim$ fF, and has been neglected in the calculations.

We have numerically solved the associated stochastic differential equation in case of a YBCO SQUID with 1 GHz drive. We have considered a symmetric YBCO SQUID with negligible capacitance. The noise source has been taken at temperature of 4.2 K. With these parameters, the dynamics of the SQUID shown in Fig. 2 is essentially identical to that without noise source.

The weakness of thermal noise is confirmed by the calculation of the Power Spectral Density (PSD) shown in Fig. 3. The spectrum is almost identical to the unperturbed one a part from a small background noise. Even at high frequency (around 500 GHz) the estimated signal to noise ratio is $\sim 10^7$.

The effect of noise is maximum when the energy barrier is shallow and undesired transitions are most likely to occur. Therefore, we expect an increased noise influence for slow frequency drive since the system remains in a shallow barrier potential for a longer time. However, even in this situation these noise effects can be reduced by increasing I_B in order to restore the privileged direction of the dynamics.

VOLTAGE SPECTRUM AND POWER

To obtain the voltage power spectrum we first calculate the Fourier transform of the voltage $V(t)$

$$V(\Omega) = \int_0^T dt e^{i\Omega t} V(t). \tag{14}$$

The power spectral density (PSD) is then

$$\mathrm{PSD}(\Omega) = \frac{1}{T}|V(\Omega)|^2. \tag{15}$$

The power P discussed in the main text is calculated by integrating the PSD around the resonances $k\nu$ (where ν is the monochromatic drive frequency) and dividing for a standard load resistance of 50 Ohm. This is the power we would measure *at a given resonance frequency* with a bandwidth exceeding the linewidth of the resonance.

With the device described above the output voltage can be easily increased by fabricating a chain of SQUIDs [11, 26, 27]. With N SQUIDs in series, the voltage drop across the chain increases linearly with N, whilst the PSD and the power P scale as N^2.